Careful analysis of the $^{40}Ar/^{36}Ar$ ratio may clarify whether the ^{40}Ar was deposited in large quantities in the past or continuously to the present. It is possible that both the ^{40}Ar and ^{36}Ar fluxes could be used to estimate the length of time a rock fragment has been on the surface and the orientations that it has had. The analysis of returned segments of a Surveyor or a lunar module may determine the present rate of ^{40}Ar deposition and show the expected variation with orientation in the $^{40}Ar/^{36}Ar$ ratio.

In conclusion, it appears that the lunar atmosphere is the likely source for the surface-correlated ^{40}Ar in the lunar soil grains. The atmosphere probably contains other elements from the lunar interior and solar wind elements, which have struck the moon and then been released. Thus the lunar atmosphere is likely to be the source of other unexpected surface elements that are not abundant in the solar wind and of solar wind elements that impinge upon the surface from non-solar wind directions.

R. H. MANKA

Space Physics Division,
Manned Spacecraft Center,
Houston, Texas 77058

F. C. MICHEL

Space Science Department,
Rice University,
Houston, Texas 77001

References and Notes

1. Theoretical considerations make a large ^{40}Ar content in the solar wind unlikely [D. D. Clayton, personal communication].
2. K. Marti, G. W. Lugmair, H. C. Urey, *Science* **167**, 548 (1970); J. G. Funkhouser, O. A. Schaeffer, D. D. Bogard, J. Zähringer, *ibid.*, p. 561.
3. D. Heymann, A. Yaniv, J. A. S. Adams, G. E. Fryer, *ibid.*, p. 555.
4. The relationship between the ^{40}Ar data and the lunar atmosphere is discussed in more detail by D. Heymann and A. Yaniv, *Geochim. Cosmochim. Acta*, in press.
5. The energy and flux of lunar ions due to these fields will be described in detail by R. H. Manka and F. C. Michel, in preparation.
6. F. C. Michel, *Planet. Space Sci.* **12**, 1075 (1964).
7. R. H. Manka and H. R. Anderson, *Trans. Amer. Geophys. Union* **50**, 217 (1969).
8. W. Bernstein, R. W. Fredericks, J. L. Vogl, W. A. Fowler, *Icarus* **2**, 233 (1963).
9. F. Bühler, J. Geiss, J. Meister, P. Eberhardt, J. C. Huneke, P. Signer, *Earth Planet. Sci. Lett.* **1**, 249 (1966).
10. R. O. Pepin, L. E. Nyquist, D. Phinney, D. C. Black, *Science* **167**, 550 (1970); D. D. Bogard, personal communication.
11. Supported in part by NASA grant NAS9-5911. We thank Dr. D. D. Clayton (Rice University) and Drs. D. D. Bogard, R. K. Jaggi and C. S. Warren (Manned Spacecraft Center) for helpful discussions; we especially thank Drs. D. Heymann and A. Yaniv (Rice University) for their helpful comments and discussions regarding their data showing the surface correlation of ^{40}Ar.

22 May 1970

Phylum Ectoprocta, Order Cheilostomata: Microprobe Analysis of Calcium, Magnesium, Strontium, and Phosphorus in Skeletons

Abstract. *Calcium, magnesium, and strontium occur in approximately constant ratios in traverses through skeletal walls of a single mineralogy (either calcite or aragonite). Skeletal walls of more than one mineralogy have the magnesium-rich layer (calcite) surrounding the living chamber and the strontium-rich layer (aragonite) on the outside. In contrast, phosphorus may be present in greater or lesser amounts in different parts of the same calcite skeletal wall. Aragonitic crystallites appear oriented roughly perpendicular to skeletal walls, whereas calcitic crystallites are parallel to skeletal walls.*

The phylum Ectoprocta (Bryozoa in part) includes 20,000 living and extinct species (*1*) and ranks as one of the more diverse groups of organisms. They are abundant in most encrusting communities. The colonies are composed of compartmentalized calcareous skeletons (Figs. 1 and 2) each of which houses a feeding polypide.

Chemical analyses, x-ray diffraction studies, and other techniques have disclosed general characteristics of elemental composition and mineralogy of the skeleton (*2, 3*). These results are most often expressed as average percentages of different elements or mineral phases. The spatial distribution of mineral phases has been observed to date by staining techniques, optical examination of thin sections, and bulk x-ray diffraction of specimens at different ontogenetic stages (*4, 5*). Greater precision and flexibility in choice of materials for determining the spatial distribution of calcite and aragonite is permitted by monitoring Sr and Mg by the electron probe in traverses of skeletal walls (Figs. 1–3). Strontium oxide (SrO) is much higher in aragonite than in calcite [1 compared to 0.3 percent (by weight) of ash], whereas MgO is an order of magnitude higher in calcite than in aragonite [3 to 4 compared to 0.3 percent (by weight) of ash] (*2*). Sr and Mg substitute for Ca in carbonates.

Two types of analysis were made with an ARL-SEM electron probe. (i) Qualitative mechanical, motor-driven traverses (16 μm/min) were made under a static beam which monitored the intensity of Ca, Mg, Sr (four species), and P (1 species) across skeletal walls of several individuals. The samples had been analyzed for their gross elemental and mineralogic composition (*2, 6*). The probe was operated at 20 kv and a 0.05-μa specimen current. (ii) A few scanning pictures were taken of Ca, Mg, Sr, and P distributions in order to map these elements in the surface area of transverse or deep tangential sections (Figs. 1–3).

The cuticular layer between calcareous walls of adjacent individuals (Fig. 2) is represented in traverses by a sharp drop in elemental concentration (best seen in Ca, Fig. 4, a, b, and e). This layer is sufficiently thin in some lateral walls so that averaging effects of the probe (over 4 to 5 μm) obscure its recognition. No definite cuticle was observed in adjacent end walls. This supports the observations that lateral walls are generally double calcified walls and that end walls are single calcified walls (*7*), and consequently that the mode of formation of these walls is quite different (*7*).

In species of single mineralogy (Fig. 4, species A and D), no significant spatial differences were found within a colony in ratios of Ca, Mg, or Sr. These elements vary to an important extent only with respect to the degree of mineralization and the type of mineralogy (calcite in species A, and aragonite in species D). However, P may vary considerably in amount in adjacent walls (Figs. 4, a and b). Colonies of species A are organized so that adjacent individuals only partly overlap (as in Fig. 2B). During growth, the early-formed part of a lateral wall is against a completely budded individual, and the later-formed part is adjacent to an incompletely budded individual. The high values for P seem to occur only in the early-formed part of the lateral wall. Thus P may be systematically enhanced and depressed in different growth stages of the same individual.

The structure of the calcified wall can be correlated with mineralogy. Species D is aragonitic, and its walls are composed of fibrils of mineral that appear to be perpendicular to, or radiating from the depositional surface. This was observed as "fans" of crys-

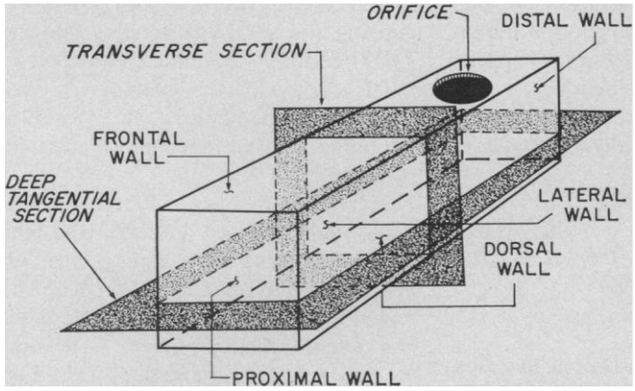

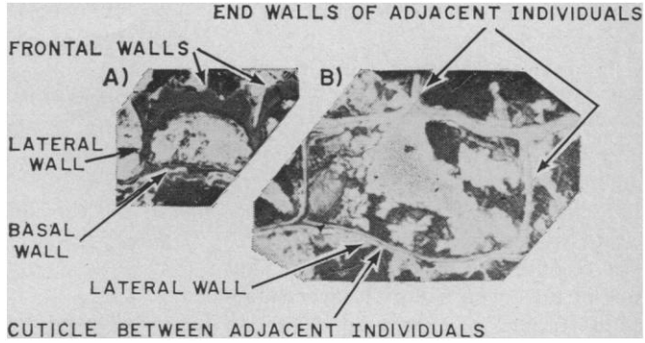

Fig. 1 (left). Sketch of calcareous skeletal box of single ectoproct individual, about 0.5 mm long, separated from a colony of thousands of similar, adjoining individuals. Traverses were taken on transverse and deep tangential sections for analysis of frontal, lateral, end (proximal and distal), and dorsal walls. Fig. 2 (right). Photographs of ground sections of ectoprocts. (A) Transverse section of species C. Most of the thick frontal wall is aragonite. (B) Deep tangential section of species B. Note the double lateral walls with the dark cuticle between calcified tissues. Individual is about 0.6 mm long.

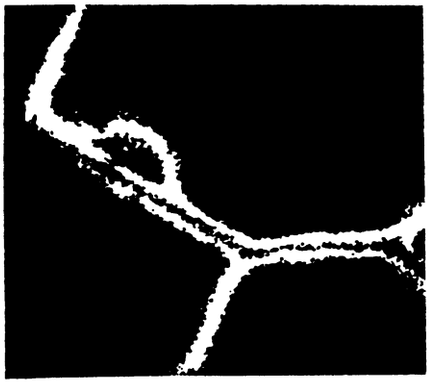

Fig. 3. X-ray image of Ca in adjacent walls of a transverse section of the ectoproct *Flustra foliacea*. The double wall of the skeleton of adjacent individuals and the outpouching "pore-chamber" are evident (about × 1000).

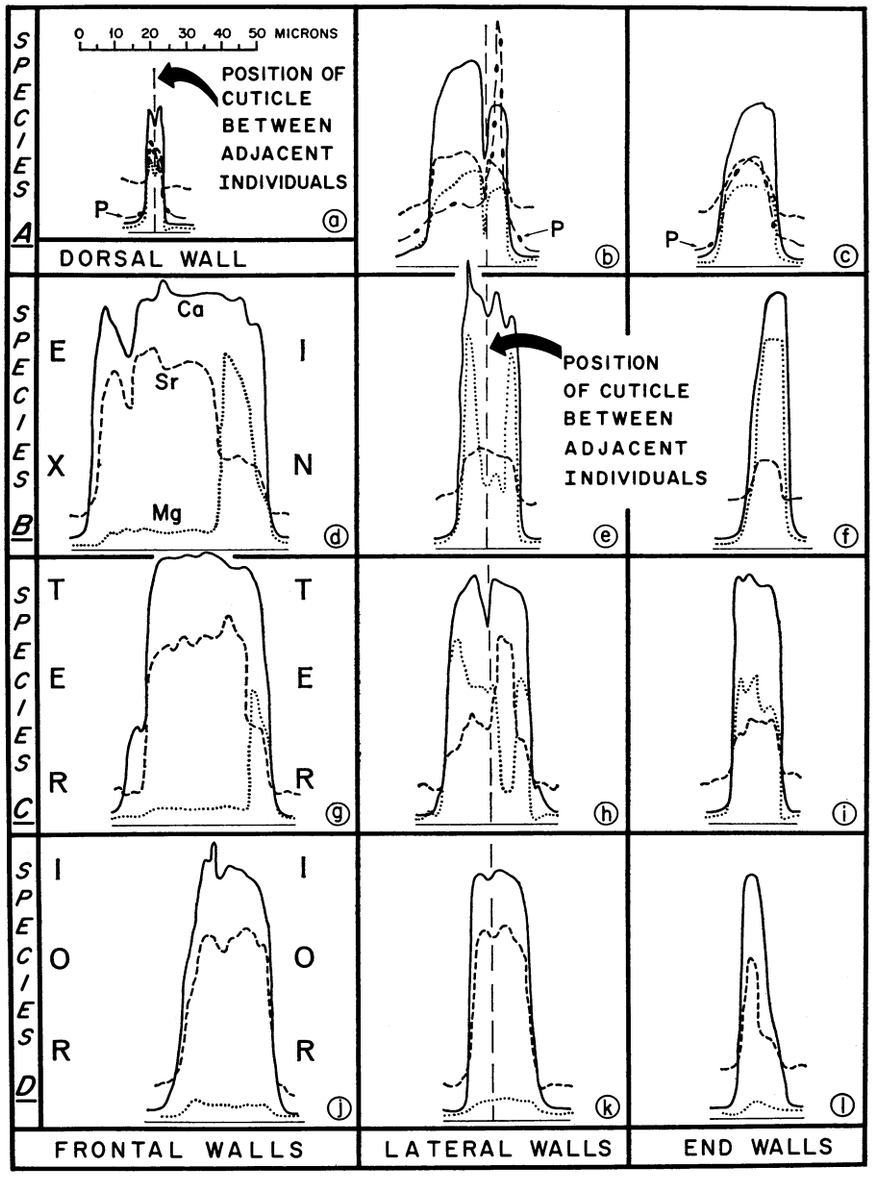

Fig. 4. *Flustra foliacea*: (a) dorsal walls of two individuals; (b) lateral walls of two individuals; (c) distal and proximal walls of two individuals. *Cryptosula pallasiana*: (d) frontal wall; (e) lateral walls of two individuals; (f) distal wall and proximal wall of two individuals. *Schizoporella unicornis*: (g) frontal wall; (h) lateral walls of two individuals; (i) distal wall and proximal wall of two individuals. *Parasmittina nitida*: (j) frontal wall; (k) lateral walls of two individuals; (l) distal and proximal walls of two individuals. Each point on the graphs represents an average of the concentration for the element through a distance of 4 to 5 μm. The vertical scale is an arbitrary, convenient representation which is different for each element, but the same for every traverse. A series of low peaks, as in (a), represents a poorly calcified skeletal wall. EXTERIOR and INTERIOR refer to the orientation of the frontal wall.

tals with the same optical orientation when viewed in crossed nicols. In contrast, species A has very thin calcitic walls in which the mineralized crystals appear to be oriented parallel to the depositional surface.

In species of more than one mineralogy (Fig. 4, species B and C), spatial differences in Sr and Mg are most apparent in the frontal wall, although differences may also occur in lateral and end walls. The skeletal layer adjacent to the internal space is rich in Mg (calcite) (Fig. 4, d and g). Outside of this layer, a Sr-rich layer (aragonite) occurs in a crust up to 30 μm thick, which confirms spatial relationships suggested by staining and other methods (*4*, *5*). This aragonitic crust extends proximally, distally, and laterally downward over the proximal, distal, and lateral calcitic walls. It does not extend to the base but rather pinches out between individuals. Thus a sequence of calcite-aragonite followed by aragonite-calcite in a traverse across lateral walls indicates that the traverse was made in the middle to upper part of the wall where the aragonitic layers of adjacent individuals were wrapping around the calcitic skeletal boxes. This wrapping around of the aragonitic layer is most evident in the right-hand individual of Fig. 4h.

The structure of the calcified wall is similar in both species with calcite and aragonite. The calcitic inner layer consists of crystallites parallel to the wall, whereas the aragonitic outer layer is composed of fibers radiating from the wall. This pattern has also been found in a species of *Metrarabdotos* that had an aragonitic outer layer and a calcitic inner layer (*4*). Perhaps the pattern of a calcitic internal lamellar layer and an aragonitic external fibrous layer is typical of ectoproct species with more than one mineralogy.

THOMAS J. M. SCHOPF
Department of the Geophysical Sciences, University of Chicago, Chicago, Illinois 60637

J. R. ALLAN
Gulf Oil Corporation, P.O. Box 1012, Houma, Louisiana 70360

References and Notes

1. L. Hyman, *The Invertebrates*, vol. 5, *Smaller Coelomate Groups* (McGraw-Hill, New York, 1959); R. S. Boardman and A. H. Cheetham, *J. Paleontol.* **43**, 205 (1969).
2. T. J. M. Schopf and F. T. Manheim, *J. Paleontol.* **41**, 1197 (1967); *ibid.* **42**, 858 (1968).
3. J. B. Rucker, *Atti Soc. Ital. Sci. Natur. Mus. Civico Storia Natur. Milano* **108**, 101 (1968); P. A. Sandberg, M. C. Moore, R. D. Stieglitz, T. R. Worsley, *Mtg. Geol. Soc. Amer., Program 1969 Southeastern Sect.*, p. 73 (1969).
4. A. H. Cheetham, J. B. Rucker, R. E. Carver, *J. Paleontol.* **43**, 129 (1969).
5. J. B. Rucker and R. E. Carver, *ibid.* **43**, 791 (1969); T. J. M. Schopf and D. F. Travis, *Biol. Bull.* **135**, 436 (1968).
6. The analyses (percent) and species used were as follows. *Flustra foliacea*: CaO, 48.8; MgO, 3.1; SrO, 0.26; P_2O_5, 0.93; calcite, 100; aragonite, 0; *Cryptosula pallasiana*: CaO, 44.4; MgO, 3.0; SrO, 0.41; P_2O_5, 0.41; calcite, 70; aragonite, 30; *Schizoporella unicornis*: CaO, 51.4; MgO, 1.9; SrO, 0.62; P_2O_5, 0.37; calcite, 50; aragonite, 50. *Parasmittina nitida*: CaO, 53.3; MgO, 0.25; SrO, 1.0; P_2O_5, 0.19, calcite, 0; aragonite, 100. Carbon dioxide accounts for most of the rest. Wet chemical and mineralogic determinations are averages from the same lots of material used for our microprobe analyses (*2*). Percentages of oxides are given as percentage (by weight) of organic-free ash (500°C).
7. W. C. Banta, *J. Morphology* **125**, 497 (1968); *Atti Soc. Ital. Sci. Natur. Mus. Civico Storia Natur. Milano* **108**, 93 (1968).
8. We thank Dr. J. Goldstein and P. LaRussa for general advice and for technical assistance in operating the probe; Dr. F. T. Manheim, Dr. Alan Cheetham, and K. W. Kaufmann, Jr., for technical review. Support provided by the Office of Research, Lehigh University, where the data were mostly obtained.

9 March 1970

Alcohol Oxidation in Rats Inhibited by Pyrazole, Oximes, and Amides

Abstract. *Pyrazole, previously reported to inhibit ethanol oxidation in the rat, also effectively blocks the in vivo metabolism of methanol, propanol, isopropanol,* n-*butanol, and isobutanol. A variety of oximes and amides are also effective inhibitors of ethanol metabolism. These various inhibitors may prove important in the elucidation of several facets of alcohol metabolism and also may have application in the treatment of methanol poisoning and in the reduction of the sequelae of the disulfiram-ethanol reaction syndrome in man.*

In 1963 Theorell and Yonetani reported that pyrazole is an inhibitor of liver alcohol dehydrogenase (ADH) in vitro (*1*). Pyrazole was shown to form a ternary complex with ADH and nicotinamide-adenine dinucleotide (NAD) with pyrazole occupying the ethanol binding site (*2*, *3*). Later, pyrazole and various 4-substituted pyrazoles were shown to inhibit ethanol oxidation in vivo whereas substitution at other than the 4-position resulted in loss of the inhibitory effect (*3–5*). In several recent studies pyrazole has been shown to be an effective in vivo inhibitor of ethanol oxidation in rats and dogs (*6*, *7*). Amides form a ternary complex with ADH and reduced NAD (NADH) in vitro with the amide occupying the aldehyde binding site (*2*, *3*). Therefore, we studied the effect of the formation of this complex in vivo on ethanol metabolism and observed inhibition with various amides and with pyrazole.

Increased amounts of blood acetaldehyde were detected in men who had ingested ethanol after having been exposed to *n*-butyraldoxime (*8*). Koe and Tenen have found that *n*-butyraldoxime is a potent inhibitor of liver ADH both in vivo and in vitro and, in addition, that there is a large decrease in liver aldehyde dehydrogenase activity in mice pretreated with *n*-butyraldoxime, an inhibition not demonstrable in vitro (*9*). Various other oximes are shown here to be equally effective inhibitors of the oxidation of ethanol and other alcohols in the rat.

In the present study we demonstrate the inhibitory action of pyrazole on a series of alcohols and document the inhibition of alcohol metabolism by various amides and oximes. We determined the rate of alcohol metabolism in fasted Sprague-Dawley rats, each weighing 175 to 225 g, by measuring the rate of disappearance of alcohol (*10*) or the rate of excretion of ^{14}C-labeled CO_2 in expired air after administration of the ^{14}C-labeled alcohol (*11*). An attempt was made to compare the relative effectiveness of these inhibitors as well as the margin of safety.

The effectiveness of pyrazole (6.6 mmole/kg) as an inhibitor of the oxidation of a series of alcohols is shown in Table 1. Oxidation of the primary alcohols proceeds at a rate of 5.8 to 7.2 mmole kg^{-1} $hour^{-1}$, except for methanol which is oxidized at about one-tenth of this rate. Although these primary alcohols are oxidized nearly equally well, pyrazole is a more effective inhibitor of ethanol oxidation than of the oxidation of the other alcohols, a relationship expected from the competition between inhibitor and substrate for ADH and the decrease of the Michaelis constant (K_m) with increase in the chain length of the alcohols (*12–14*). That the inhibition occurs at the first stage of the oxidation of the alcohol is shown by the inhibition of ADH in vitro and the fact that acetate metabolism is not inhibited after administration of pyrazole. The rate of metabolism of [1-^{14}C]acetate (10 mmole/kg) was 4.19 mmole kg^{-1}